# Dissection of Three Ca$^{2+}$-Dependent Steps Leading to Secretion in Chromaffin Cells from Mouse Adrenal Slices

Thomas Voets*
Department of Membrane Biophysics
Max Planck Institute for Biophysical Chemistry
Am Fassberg 11
D-37077 Göttingen
Germany

## Summary

In neurosecretory cells, intracellular Ca$^{2+}$ ([Ca$^{2+}$]$_i$) not only acts as the trigger for secretion but also regulates earlier steps in the secretory pathway. Here, a novel approach was developed to control [Ca$^{2+}$]$_i$ over a broad concentration range, which allowed the quantification of three distinct actions of [Ca$^{2+}$]$_i$ on large dense-core vesicle (LDCV) fusion in chromaffin cells from mouse adrenal slices. Basal [Ca$^{2+}$]$_i$ regulated the transfer of vesicles toward a slowly releasable state, whereas further maturation to the readily releasable state was Ca$^{2+}$ independent. [Ca$^{2+}$]$_i$ levels above 3 $\mu$M triggered exocytosis of all readily and slowly releasable vesicles in two parallel, kinetically distinct fusion reactions. In a molecular context, these results suggest that Ca$^{2+}$ acts both before and after trans-SNARE complex formation to regulate fusion competence and fusion kinetics of LDCVs.

## Introduction

At any given time, only a subset of all vesicles in a neurosecretory cell is available for rapid secretion. These release-ready vesicles differ from the bulk of vesicles by the fact that they are closely attached to the target membrane ("docked") and have undergone maturation ("priming"), such that they only need the final trigger, an elevation of [Ca$^{2+}$]$_i$, to undergo fusion. Immediately after intense stimulation, the readily releasable pool of vesicles (RRP) may be partially or fully depleted, causing a period of secretory depression until the RRP is refilled. The processes of RRP depletion and refilling are believed to play a major role in short-term plasticity in many neurosecretory cells (reviewed in Zucker, 1996; Neher, 1998).

Besides its established role as trigger for vesicle fusion, elevated [Ca$^{2+}$]$_i$ has been proposed to accelerate the transfer of vesicles to the RRP. Kusano and Landau (1975) found that the supply of releasable vesicles at the squid giant synapse was accelerated during high-frequency stimulation and discussed the possibility that this was due to the increase in [Ca$^{2+}$]$_i$. This hypothesis has been confirmed in more recent reports in chromaffin cells (Bittner and Holz, 1992; von Rüden and Neher, 1993; Smith et al., 1998) and different neuronal synapses (Dittman and Regehr, 1998; Stevens and Wesseling, 1998; Wang and Kaczmarek, 1998; Gomis et al., 1999),

suggesting that Ca$^{2+}$-dependent vesicle maturation is a general property of neurosecretion.

The precise molecular mechanisms whereby Ca$^{2+}$ regulates the supply of fusion-competent vesicles and triggers exocytosis remain elusive. Nevertheless, a large number of proteins have been identified that are supposedly involved in critical steps leading to membrane fusion (for a recent review, see Augustine et al., 1999; Fernandez-Chacon and Südhof, 1999). Probably the best-characterized components of the exocytic machinery are the SNARE proteins: syntaxin, SNAP-25, and synaptobrevin. These proteins are able to form a trans-SNARE complex, thereby bringing vesicle and target membrane in close apposition (Sutton et al., 1998). While the importance of these proteins in neurosecretion is beyond doubt, there is conflicting evidence concerning the relative timing of trans-SNARE complex formation and Ca$^{2+}$-triggered membrane fusion. Recent experiments performed in permeabilized PC12 cells showed that monomeric SNAREs and Ca$^{2+}$ are required simultaneously for exocytosis to occur (Chen et al., 1999; Scales et al., 2000). This data led to the conclusion that Ca$^{2+}$ triggers trans-SNARE complex formation and thereby drives membrane fusion. In contrast, studies in chromaffin cells and rat synaptosomes showed that manipulations influencing SNARE complex formation affected the supply of release-ready vesicles but not the final fusion step (Xu et al., 1999; Lonart and Südhof, 2000; Wei et al., 2000), indicating that SNARE complexes form before Ca$^{2+}$-triggered exocytosis. It is well possible that these apparent contradictions originate, at least partially, from difficulties in making a clear distinction between Ca$^{2+}$-dependent vesicle maturation and Ca$^{2+}$-dependent fusion.

Here, a method was developed that allows the dissection and quantitative description of different Ca$^{2+}$-dependent steps leading to LDCV fusion in chromaffin cells from mouse adrenal slices. The range of Ca$^{2+}$ measurements was extended by using a mixture of the high-affinity dye Fura-2 (Grynkiewicz et al., 1985) and the low-affinity dye Furaptra (Konishi et al., 1991). These two ratiometric Ca$^{2+}$ indicators display similar fluorescence properties but differ in their Ca$^{2+}$ binding affinity by a factor of about 100. The combined use of these dyes enabled accurate measurement of [Ca$^{2+}$]$_i$ from the nanomolar range up to about 300 $\mu$M. To achieve optimal control of [Ca$^{2+}$]$_i$ at its sites of action, spatially uniform changes in [Ca$^{2+}$]$_i$ were induced by photolysing the photolabile Ca$^{2+}$ chelator nitrophenyl-EGTA (NP-EGTA). Low-intensity steady-light illumination was used to create moderate increases in basal [Ca$^{2+}$]$_i$, whereas short intense light flashes causing stepwise increases in [Ca$^{2+}$]$_i$ to above 3 $\mu$M were applied to trigger secretion. The exclusive use of Ca$^{2+}$ uncaging circumvented uncertainties about the time course and spatial pattern of the intracellular Ca$^{2+}$ signal, which are known to complicate the interpretation of data obtained with electrical and/or pharmacological stimulation (Neher, 1998). High time resolution capacitance measurements of the secretory response to flashes allowed the precise determina-

* E-mail: tvoets@gwdg.de
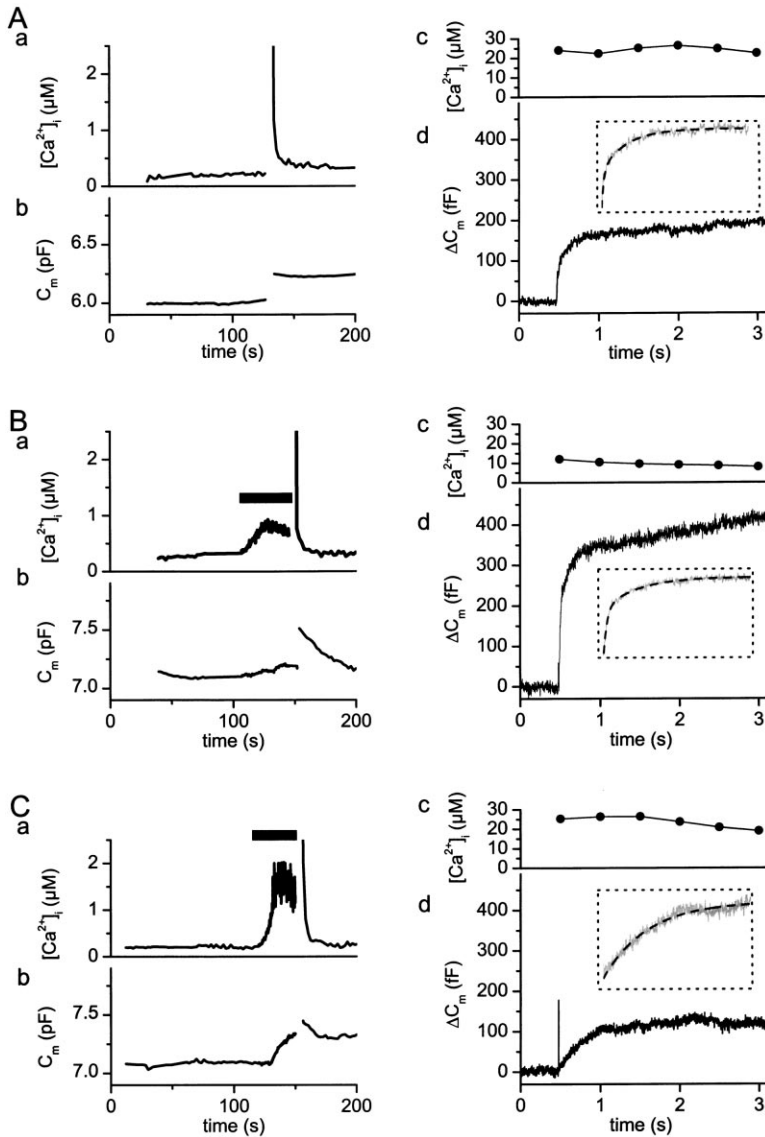
Figure 1. Capacitance Responses to Flash Photolysis of Caged Ca²⁺ from Three Different Basal Ca²⁺ Levels

Three representative examples (A–C) illustrate the experimental procedure that was used to determine the Ca²⁺ dependence of the amount of vesicles in the slowly releasable pool (SRP) and readily releasable pool (RRP). ([a] and [b] in [A]–[C]) Simultaneous measurements of intracellular Ca²⁺ ([Ca²⁺]$_i$) and membrane capacitance (C$_m$) at low time resolution. In these panels, time zero corresponds to the point at which the whole cell configuration was established. The gap in the traces corresponds to the period during which a flash was applied and both [Ca²⁺]$_i$ and C$_m$ were measured at high time resolution, as shown in (c) and (d) in (A)–(C). Bars in (Ba) and (Ca) correspond to periods during which the durations of the UV illumination episodes from the monochromator were prolonged, causing a spatially homogeneous increase in [Ca²⁺]$_i$ before the flash. ([d] in [A]–[C]) The insets show the first second of the flash response. Superimposed is the double exponential fit that was used to determine the amplitude and time constant of both kinetic components of the exocytic bursts.

tion of the sizes and fusion kinetics of two distinct pools of releasable vesicles, the slowly releasable pool (SRP) and the RRP (Voets et al., 1999). These vesicle pools are thought to contain those vesicles that are connected to the plasma membrane through *trans*-SNARE complexes. The transition between both SRP and RRP, which occurs on the seconds scale, may correspond to the interconversion of the SNARE complex between a loose to a tight state (Voets et al., 1999; Xu et al., 1999).

Using this novel approach, three conclusions were reached: (1) [Ca²⁺]$_i$ accelerates the supply of vesicles toward the SRP but does not affect the further transition to the RRP, (2) sustained [Ca²⁺]$_i$ levels above 3 μM trigger the fusion of all vesicles in the RRP and SRP, and (3) the fusion of vesicles from SRP and RRP occurs in two parallel reactions exhibiting distinct Ca²⁺ binding properties. A quantitative model is presented that correlates the three observed actions of [Ca²⁺]$_i$ with results from earlier studies on the role of SNARE complex assembly in LDCV secretion.

## Results

Figure 1 shows three examples of the applied experimental procedure used to determine the influence of basal [Ca²⁺]$_i$ on the amount of release-ready vesicles. Chromaffin cells in situ were loaded through the patch pipette with a solution containing two ratiometric Ca²⁺ indicator dyes, Fura-2 and Furaptra, as well as the photolabile Ca²⁺ chelator NP-EGTA, partially loaded with Ca²⁺. In all three examples, the initial [Ca²⁺]$_i$ value was ∼200 nM, as estimated from the ratio of the fluorescence signals measured during short (15 ms) and low-frequency (0.5 Hz) illuminations at 350 and 380 nm (Figures 1Aa, 1Ba, and 1Ca). About 130 s after the start of the experiment shown in Figure 1A, a flash was applied, causing a rapid uniform increase in [Ca²⁺]$_i$ to ∼25 μM (Figure 1Ac). The flash-induced increase in membrane capacitance (C$_m$) consists of a rapid exocytic burst, followed by a slower sustained phase of secretion (Figure 1Ad; see Heinemann et al., 1994; Voets et al., 1999).
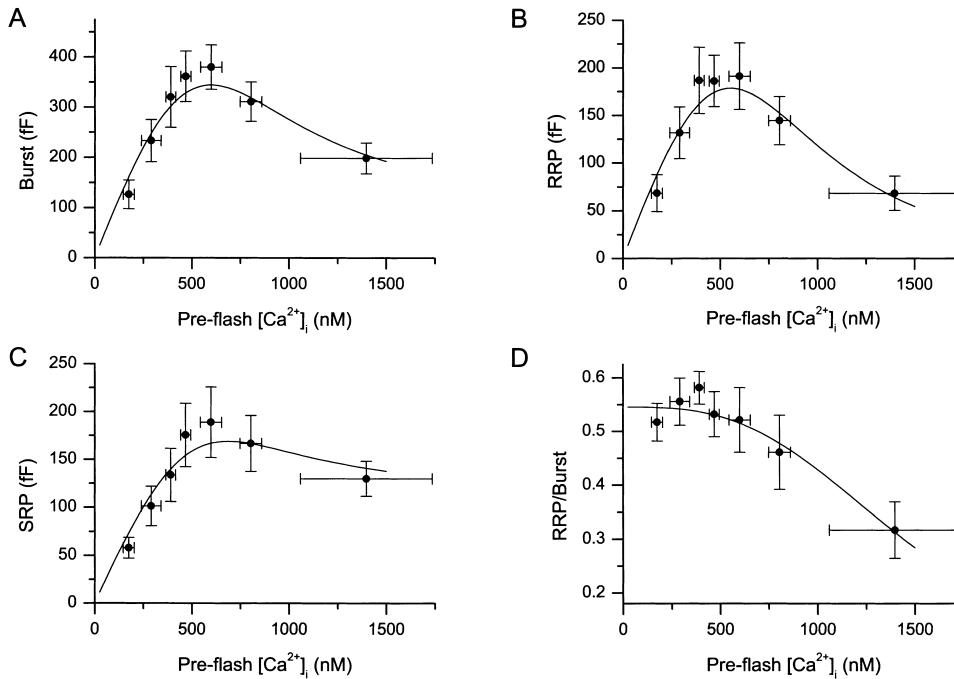
Figure 2. Basal $[Ca^{2+}]_i$ Regulates the Size of SRP and RRP

(A) $Ca^{2+}$ dependence of the amplitude of the exocytic burst, defined as the sum of the amplitudes of both kinetics components obtained from double exponential fits. Experiments (71) were analyzed and binned according to the averaged $[Ca^{2+}]_i$ in a 30 s period preceding the flash (8 to 13 cells per bin).

(B) $Ca^{2+}$ dependence of the size of the RRP, which was determined as the amplitude of the fast kinetic component obtained from the double exponential fits to the exocytic bursts.

(C) $Ca^{2+}$ dependence of the size of the SRP, which was determined as the amplitude of the slow kinetic component obtained from the double exponential fits to the exocytic bursts.

(D) RRP sizes were normalized to the amplitude of full exocytic bursts and plotted versus preflash $[Ca^{2+}]_i$.

Solid lines in (A)–(D) represent the predictions of the model shown in Figure 6.

The exocytic burst can be fitted by the sum of two exponential terms, with the fast and slower component corresponding to the fusion of vesicles from the RRP and SRP, respectively (Voets et al., 1999). Applying double exponential fitting to the example of Figure 1A yields an RRP size of 88 fF, with a fusion rate constant of 60 $s^{-1}$, and an SRP size of 75 fF, with a fusion rate constant of 5.8 $s^{-1}$ (Figure 1Ad, inset). To examine the effect of increased basal $[Ca^{2+}]_i$ on the availability and distribution of fusion-competent vesicles, the frequency of the illuminations at 350 and 380 nm was increased (thick bars in Figures 1Ba and 1Ca). The resulting photolysis of moderate amounts of NP-EGTA leads to an elevated $[Ca^{2+}]_i$ level before the flash. In the experiment shown in Figure 1B, $[Ca^{2+}]_i$ was raised to ~700 nM before the flash, which resulted in a robust exocytic burst. Double exponential fitting revealed an RRP size of 206 fF and an SRP size of 150 fF, with fusion rate constants of 55 $s^{-1}$ and 5.9 $s^{-1}$, respectively. At a preflash $[Ca^{2+}]_i$ of ~1500 nM (Figure 1C), the subsequent flash resulted in a small, monoexponential exocytic burst. The slowness of the rate constant (4.8 $s^{-1}$) indicates that this burst corresponds to the fusion of vesicles from an SRP of 117 fF and that the RRP size is negligible in this example.

Figure 2 summarizes data from 71 similar experiments, in which $[Ca^{2+}]_i$ before the flash ranged from 150 to 1600 nM. At concentrations below 600 nM, $[Ca^{2+}]_i$ caused an increase in the size of the exocytic burst, which reached a maximum of 380 ± 44 fF at $[Ca^{2+}]_i$ of 598 ± 55 nM (Figure 2A). The growth of the exocytic burst was due to a parallel augmentation in the size of SRP and RRP (Figures 2B–2C), and the relative contribution of the RRP to the exocytic burst remained fairly constant (Figure 2D). This indicates that the equilibrium between SRP and RRP, which occurs on the seconds timescale (Voets et al., 1999), is not influenced by $[Ca^{2+}]_i$ in this concentration range. At higher $[Ca^{2+}]_i$ levels, a pronounced decrease in RRP size and a more moderate reduction of the SRP was observed. This decrease in the amount of releasable vesicles coincided with clear indications of exocytosis already, before delivery of the flash (see Figure 1Cb), indicating that releasable vesicles are lost through exocytosis at these elevated $[Ca^{2+}]_i$ concentrations. Note that the significant decrease of the relative contribution of the RRP to the exocytic burst observed at $[Ca^{2+}]_i > 600$ nM (Figure 2D) does not imply that $[Ca^{2+}]_i$ influences the equilibrium between SRP and RRP. As shown below, the $Ca^{2+}$ dependence of the ratio RRP/burst can be completely accounted for by the different $Ca^{2+}$ dependence of the fusion reactions from SRP and RRP.

Next, we examined how the size of the components of the exocytic burst is affected by postflash $[Ca^{2+}]_i$. If, as proposed in our previous work (Voets et al., 1999),
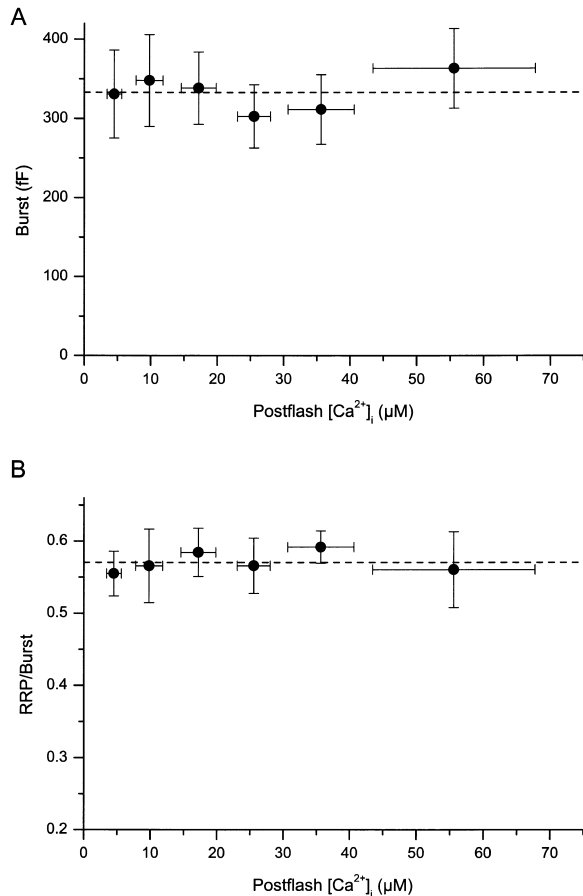
**Figure 3. The Size of the Exocytic Burst and Its Components Do Not Depend on Postflash [Ca$^{2+}$]$_i$**

(A) The measured amplitudes of the exocytic burst were pooled for 51 cells with basal [Ca$^{2+}$]$_i$ levels between 300 and 750 nM and binned according to the postflash [Ca$^{2+}$]$_i$. The dotted line corresponds to the average burst amplitude (333 fF) for these cells.

(B) The contribution of the fast component (RRP) to the exocytic burst was determined for the same 51 cells as in (A). The dotted line corresponds to the average contribution (0.57) for these cells.
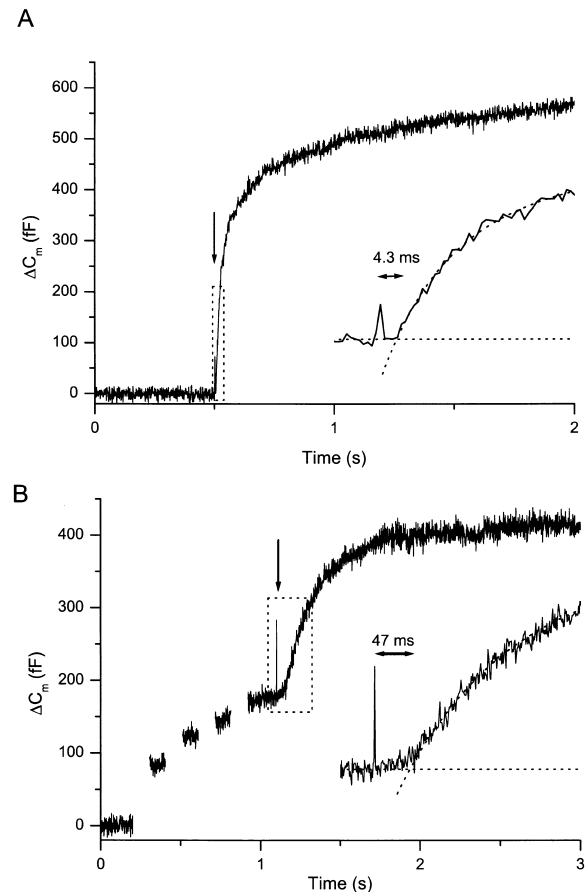


**Figure 4. Determination of the Exocytic Delay**

(A) A representative flash response illustrating the procedure for determining the exocytic delay for fusion from the RRP. The rising phase of the C$_m$ trace was fitted with a double exponential curve. The exocytic delay was determined as the time interval between the flash (arrow) and the time point at which the fitted curve crosses the preflash C$_m$ level (inset). From this value, 600 $\mu$s was subtracted to account for the delay introduced by the flash time course and the time required for calcium to be released from the NP-EGTA. In this example, postflash [Ca$^{2+}$]$_i$ was 12 $\mu$M.

(B) To determine the exocytic delay for fusion from the SRP, the flash was preceded by a train of four 100 ms depolarizations to −5 mV, which eliminates the fast component in the flash response (see Voets et al., 1999). The exocytic delay was then obtained by a similar procedure as in (A), although a single exponential was sufficient to describe the rising phase of the C$_m$ trace (inset). In this example, postflash [Ca$^{2+}$]$_i$ was 18 $\mu$M.

the exocytic burst reflects the parallel fusion of all the vesicles from SRP and RRP, postflash [Ca$^{2+}$]$_i$ is not expected to affect the amplitudes of the two kinetic components of the burst. Figure 3 shows that this is indeed the case; both the amplitude of the exocytic burst (Figure 3A) and the relative contribution of the fast kinetic component (Figure 3B) are independent of postflash [Ca$^{2+}$]$_i$ in the range between 3 and 60 $\mu$M. This is in line with results obtained in pituitary melanotrophs (Thomas et al., 1993) and allows the exclusion of models in which the Ca$^{2+}$ sensitivity of individual vesicles is heterogeneous, as has been proposed for cortical vesicle fusion in sea urchin eggs (Vogel et al., 1996; Blank et al., 1998).

There was always a brief delay between the flash and the onset of the C$_m$ rise. This exocytic delay, defined as the time point where a double exponential fit reaches the preflash C$_m$ level (Figure 4A), decreased with increasing postflash [Ca$^{2+}$]$_i$ from ∼20 ms to less than 1 ms (Figure 5A). This is consistent with the notion that the exocytic delay reflects the binding kinetics of Ca$^{2+}$ to the Ca$^{2+}$ sensing sites on the fusion machinery (Heidelberger et al., 1994; Heinemann et al., 1994). By depleting the RRP before the flash, which can be achieved by applying a train of four 100 ms depolarizations (Figure 4B; see also Voets et al., 1999), fusion from the SRP was studied in isolation. Interestingly, in such experiments, approximately 10-fold longer exocytic delays were observed, ranging from 150 ms at 10 $\mu$M to 10 ms at 100 $\mu$M [Ca$^{2+}$]$_i$ (Figure 5A). In Figure 5B, the fast and slow rate constant of the burst were plotted against postflash [Ca$^{2+}$]$_i$. Both rate constants increased over two to three orders of magnitude with increasing [Ca$^{2+}$]$_i$, and the difference between both fusion rate constants remained fairly constant over this [Ca$^{2+}$]$_i$ range.
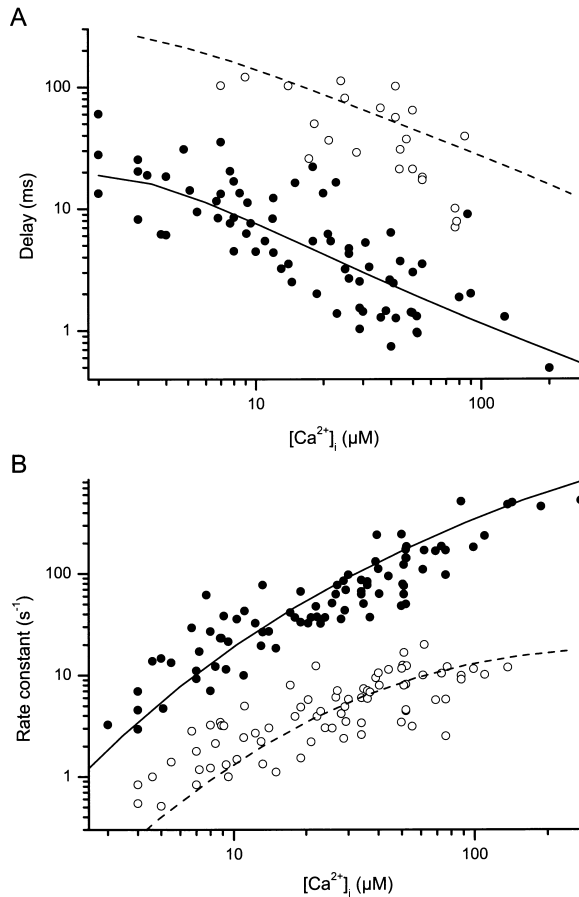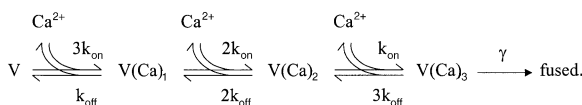
Figure 5. Ca²⁺ Dependence of the Rate Constants and Exocytic Delays for Fusion from RRP and SRP

(A) Synaptic delays for the fast component (filled circles) and the slow component (open circles), determined as explained in Figure 4.

(B) Rate constants for the fast (filled circles) and slow (open circles) component of the burst, as obtained by double exponential fitting. The solid and dotted lines in (A) and (B) correspond to the best fit with the kinetic scheme described in the text. The resulting rate constants are given in the Results section.

The kinetics of Ca²⁺-dependent exocytosis in neurosecretory cells have been generally modeled with simple linear schemes in which a number of reversible Ca²⁺ binding reactions precede an irreversible fusion reaction (reviewed in Kasai, 1999). To test whether such schemes could be applied to the fusion of vesicles from the SRP and RRP, the first-order differential equations derived from the reaction scheme were solved numerically, enabling the determination of the theoretical rates and delays. A simplex algorithm was then used to obtain constants that produced the best fit to the experimental data. It was found that for both fusion reactions at least three Ca²⁺ binding steps had to be assumed to obtain satisfactory fits to both exocytic delays (Figure 5A) and rate constants (Figure 5B). This corresponds to the following kinetic scheme:

$$V \underset{k_{off}}{\overset{3k_{on}}{\rightleftharpoons}} V(Ca)_1 \underset{2k_{off}}{\overset{2k_{on}}{\rightleftharpoons}} V(Ca)_2 \underset{3k_{off}}{\overset{k_{on}}{\rightleftharpoons}} V(Ca)_3 \overset{\gamma}{\longrightarrow} fused.$$

The best fit for the fusion of vesicles from the RRP was obtained assuming a Ca²⁺ binding rate constant ($k_{on,r}$) of $4.4 \times 10^6$ M⁻¹s⁻¹, a Ca²⁺ dissociation rate constant ($k_{off,r}$) of 56 s⁻¹, and a rate constant for the irreversible fusion reaction ($\gamma_r$) of 1450 s⁻¹. From these constants, the affinity of a single Ca²⁺ binding site can be determined as the ratio $k_{off,r}/k_{on,r}$, which yields a $K_D$ of 12.7 μM. The Ca²⁺ binding and unbinding rate constants, as well as the rate constant for the irreversible fusion reaction, had to be reduced more than 10-fold to obtain a good agreement with the experimental data for the fusion of vesicles from the SRP. The best fit to the data yielded $k_{on,s} = 0.5 \times 10^6$ M⁻¹s⁻¹, $k_{off,s} = 4$ s⁻¹, and $\gamma_s = 20$ s⁻¹, corresponding to a $K_D$ for a single Ca²⁺ binding site of 8.0 μM. These slow binding and unbinding kinetics of Ca²⁺ and the resulting long exocytic delays explain our previous finding that depolarizations lasting up to 100 ms, which can almost fully deplete the RRP, cause hardly any secretion from the SRP (Voets et al., 1999). Moreover, this detailed kinetic analysis clearly demonstrates that vesicles from SRP and RRP undergo exocytosis in two distinct fusion reactions, involving the binding of Ca²⁺ to sensors with significantly different Ca²⁺ binding kinetics.

## Discussion

In the present study, an approach was introduced that allowed the discrimination and quantitative analysis of the different Ca²⁺-dependent steps leading to LDCV fusion in mouse chromaffin cells from adrenal slices. By combining flash and steady-light photolysis of caged Ca²⁺ with [Ca²⁺]$_i$ measurements using a mixture of a low- and a high-affinity ratiometric Ca²⁺ indicator, an accurate control of [Ca²⁺]$_i$ at its sites of action was achieved over a broad concentration range. The exclusive use of Ca²⁺ uncaging to shape the intracellular Ca²⁺ signal, both before and during stimulation of exocytosis, efficiently avoided uncertainties about the time course and spatial pattern of [Ca²⁺]$_i$. In conjunction with high time resolution membrane capacitance measurements, three different Ca²⁺-dependent steps could be distinguished and quantitatively described. [Ca²⁺]$_i$ accelerates an early step in the supply of fusion-competent vesicles and triggers fusion from two distinct releasable pools with different kinetics.

### Model for the Last Steps in LDCV Fusion
The present findings can be correlated with results from earlier studies, leading to a detailed model for the last steps leading to LDCV secretion (Figure 6). The model depicts the fusion-competent vesicles (i.e., SRP and RRP) as those vesicles connected to the plasma membrane through *trans*-SNARE complexes. This view is based on studies showing that manipulations that influence formation of SNARE complexes affect the supply of release-ready vesicles rather than their fusion kinetics (Xu et al., 1999; Lonart and Südhof, 2000; Wei et al., 2000). The transition between SRP and RRP occurs with a time constant of about 4 s (Voets et al., 1999) and correspond to the interconversion between a loose and a tight state of the *trans*-SNARE complex (Xu et al., 1999). The data presented here strongly indicate that
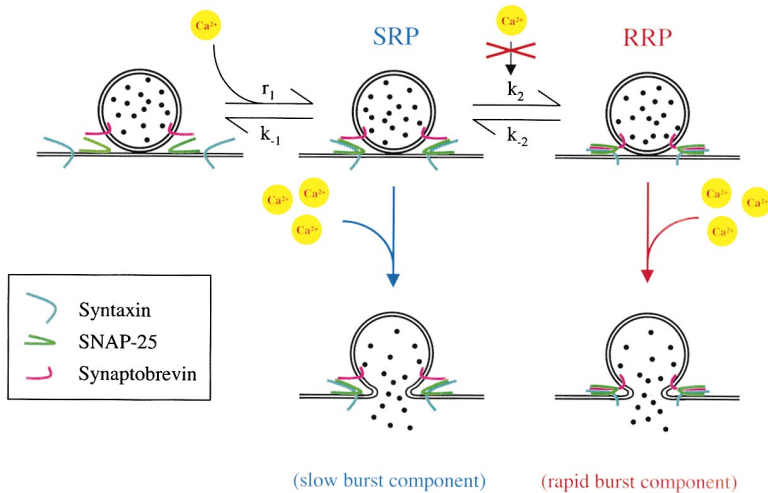
**Figure 6. Model Describing the Action of Ca²⁺ in LDCV Secretion**

Two pools of releasable vesicles are considered, termed the SRP and the RRP. These vesicles are connected to the plasma membrane by preformed *trans*-SNARE complexes in a loosely (SRP) or tightly (RRP) bound state (Xu et al., 1999). The equilibrium between SRP and RRP occurs on the seconds timescale (Voets et al., 1999) and is $Ca^{2+}$ independent. Vesicles from the SRP and RRP can both undergo exocytosis upon binding of three $Ca^{2+}$ ions, but fusion from the SRP is approximately 10-fold slower than from the RRP. A third $Ca^{2+}$-dependent step is the transition of docked but unprimed vesicles to the SRP and involves the formation of SNARE complexes from monomers. This rate of vesicles transition to the SRP is assumed to obey a Michaelis-Menten type of regulation by $[Ca^{2+}]_i$:

$$r_1 = \frac{r_{max}[Ca^{2+}]_i}{[Ca^{2+}]_i + K_D}$$

where $r_{max}$ represents the maximal rate of vesicle supply at high $[Ca^{2+}]_i$ and $K_D$ the apparent $Ca^{2+}$ affinity of a putative regulatory site. Combining values for $r_{max}$ and $K_D$ with the parameters on the $Ca^{2+}$ dependence of the fusion reactions and previously published values ($k_{-1} = 0.05$ s$^{-1}$, $k_2 = 0.12$ s$^{-1}$ and $k_{-2} = 0.1$ s$^{-1}$; see Voets et al., 1999), steady-state sizes of SRP and RRP at different $[Ca^{2+}]_i$ can be determined analytically. The best agreement between our data in Figure 2 and the model predictions was obtained with $r_{max} = 55$ fF s$^{-1}$ and $K_D = 2.3 \times 10^{-6}$ M.

this transition is $Ca^{2+}$ independent. At basal $[Ca^{2+}]_i$ levels below ~600 nM, both the SRP and the RRP increase in size with increasing $[Ca^{2+}]_i$, but their relative contributions to the exocytic burst remain unaltered. At higher basal $[Ca^{2+}]_i$, the size of the RRP declines stronger than the size of the SRP, but this can be fully accounted for by the higher rate of exocytosis from the RRP. Indeed, the fusion parameters determined in Figure 5 accurately predict the downward slopes of the relationship between basal $[Ca^{2+}]_i$ and the size of the RRP and SRP (Figure 2), which result from fusion of readily releasable vesicles at elevated basal $[Ca^{2+}]_i$.

Fusion from the SRP and RRP is shown to occur through two parallel exocytic reactions, both of which require binding of (at least) three $Ca^{2+}$ ions. In previous studies, it could not be determined whether fusion from the SRP occurs directly or indirectly, after a $Ca^{2+}$-dependent transition through the readily releasable state (Voets et al., 1999; Xu et al., 1999). Here, a combination of depolarizations and flash photolysis allowed the separate study of both components of the exocytic burst, which revealed major quantitative differences between the kinetics and $Ca^{2+}$ dependence of the fusion reaction from the SRP and the RRP. Moreover, the relative contribution of SRP and RRP was shown to be independent of postflash $[Ca^{2+}]_i$. Taken together, these data strongly suggest that vesicles in the SRP are indeed fusion competent and fuse via a pathway that does not involve a transition to the RRP.

The model attributes the observed $Ca^{2+}$-dependent increase in the size of SRP and RRP to an acceleration of the transition of vesicles from a pool of morphologically docked but fusion-incompetent vesicles to the SRP. Two earlier observations support this view. (1) An electron microscopy study in isolated chromaffin cells showed that increased basal $Ca^{2+}$ did not increase the amount of vesicles close to the plasma membrane, implying that $[Ca^{2+}]_i$ has no major effect on LDCV docking

(Plattner et al., 1997). (2) Under control conditions, fusion-competent vesicles represent only a fraction of the morphologically docked vesicles in chromaffin cells, suggesting that priming is a limiting factor in LDCV secretion (Ashery et al., 2000). A good quantitative description of the $Ca^{2+}$ dependence of the SRP and RRP sizes (Figure 2) was obtained assuming a Michaelis-Menten type of regulation of the rate of vesicle supply to the SRP by $[Ca^{2+}]_i$ (see legend to Figure 6 for details).

Note that the $Ca^{2+}$-dependent transition to the SRP is depicted to coincide with the formation of *trans*-SNARE complexes. This idea is consistent with recent work in permeabilized PC12 cells (Chen et al., 1999), showing that SNARE constituents and $Ca^{2+}$ are required simultaneously for LDCV exocytosis to occur. However, the biochemical assay used by Chen et al. (1999) did not allow the discrimination between $Ca^{2+}$-dependent priming and fusion steps. According to the present findings, the $Ca^{2+}$ trigger used in these PC12 experiments (3 μM; Chen et al., 1999) would lead both to the transfer of unprimed vesicles into the releasable pools and to their subsequent fusion.

## Potential Molecular Effectors for the Different Actions of Ca²⁺

Several different biochemical and genetic approaches over the last decades have revealed a vast amount of proteins and molecular complexes implicated in vesicle trafficking and neurosecretion (for recent reviews, see Augustine et al., 1999; Fernandez-Chacon and Südhof, 1999). However, an exact functional assignment is still missing for most of these proteins. The quantitative data presented here may help in correlating synaptic proteins—many of which contain (putative) $Ca^{2+}$ binding regions—with specific $Ca^{2+}$-dependent steps in the secretory pathway.

The results presented in this work indicate that fusion from both SRP and RRP involves binding of three $Ca^{2+}$
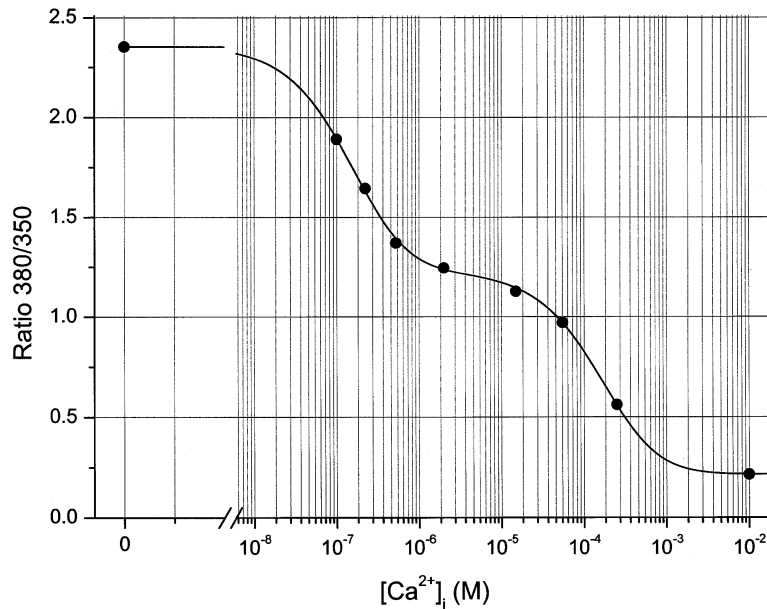
Figure 7. In Vivo Calibration Curve for a Fura-ptra-Fura-2 Mix

In vivo ratios of the fluorescent signal during illumination at 380 and 350 nm were measured using pipette solutions with $[Ca^{2+}]_i$ buffered to the indicated concentrations (see Experimental Procedures). Each data point represents the average of three to five experiments; error bars are smaller than the symbols. The experimental data were well described by a curve of the form:

$$R = R_0 - R_1 \frac{[Ca^{2+}]}{[Ca^{2+}] + K_1}$$

$$- R_2 \frac{[Ca^{2+}]}{[Ca^{2+}] + K_2}$$

where $R_0$ represents R at $[Ca^{2+}]_i = 0$ (40 mM BAPTA, no $CaCl_2$), and $(R_0 - R_1 - R_2)$ corresponds to the ratio measured with a pipette solution containing 10 mM $CaCl_2$ without any BAPTA or DPTA (solid line).

ions to sites with a $K_D$ of ~10 μM. Therefore, a possible Ca²⁺ sensor for chromaffin LDCV exocytosis may be synaptotagmin I, a Ca²⁺ binding vesicle protein for which Ca²⁺ affinities in the range between 6 and 60 μM have been reported (Brose et al., 1992; Davis et al., 1999). Synaptotagmin I has been proposed as the major Ca²⁺ sensor for synchronous neurotransmitter release in hippocampal neurons (Geppert et al., 1994) and is expressed in chromaffin cells as well (Marqueze et al., 1995). It should be noted, however, that the published rate constant for the binding of Ca²⁺ to the C₂A domain of synaptotagmin I in vitro (Davis et al., 1999) is at least one order of magnitude higher than the estimated Ca²⁺ binding rates for fusion estimated in the present work. Other potential Ca²⁺ sensors include the protein CAPS (Walent et al., 1992), other members of the synaptotagmin family (Li et al., 1995), and putative Ca²⁺ binding sites on the SNARE complex itself (Fasshauer et al., 1998). Interestingly, the estimated Ca²⁺ binding and unbinding rate constants for fusion from SRP were found to be one order of magnitude slower than for fusion from the RRP. These significant differences in Ca²⁺ binding kinetics may indicate that vesicles with loose and tight SNARE complexes utilize a different Ca²⁺ sensor for fusion. Alternatively, the conversion between the tight and loose conformation of the SNARE complex may affect the properties of the Ca²⁺ sensor, as is expected for Ca²⁺ binding sites located on the complex itself (Fasshauer et al., 1998).

The present data indicate that $[Ca^{2+}]_i$ in the submicromolar range regulates the supply of fusion-competent vesicles at a step that seems to correlate with the assembly of the *trans*-SNARE complex. This could point to a Ca²⁺-dependent action on proteins that modulate complex formation by interacting with the different SNARE constituents. For example, Munc-13-1 has been shown to play an essential role in priming of glutamatergic synaptic vesicles, possibly by interacting with the SNARE protein syntaxin (Augustin et al., 1999; Brose et al., 2000). However, LDCV secretion was found to be normal in chromaffin cells from Munc-13-1 knockout mice (T. V. and N. Brose, unpublished data). Smith et al. (1998) found that the accelerated vesicle recruitment observed at $[Ca^{2+}]_i > 450$ nM in chromaffin cells partially depended on activation of protein kinase C (PKC). The contribution of PKC activity in the present experiments should, however, be small, since pool size estimates were made less than 40 s after the elevations of basal $[Ca^{2+}]_i$. In contrast, an estimated 120 s were shown to be required for the Ca²⁺-induced activation of PKC (Smith, 1999).

## Conclusion

In this work, a novel approach was introduced to dissect and quantify different actions of Ca²⁺ on secretion from chromaffin cells in mouse adrenal slices. Since this preparation allows the direct comparison of the secretory behavior in wild-type and knockout mice, the approach and findings presented in the present work may serve as the basis for future studies examining the precise molecular mechanisms of Ca²⁺-dependent exocytosis.

## Experimental Procedures

### Adrenal Slice Preparation

Adrenal glands from 4- to 8-week-old NMRI mice were used. Slices (120–170 μm thick) were prepared as previously described (Moser and Neher, 1997). Slices were used, starting shortly after cutting, for 6–8 hr.

### Whole-Cell Capacitance Measurements

For recording, slices were fixed in the recording chamber by means of a grid of nylon threads. After mounting onto the stage of an upright microscope (Axioscope, Zeiss), the chamber was perfused at a flow rate of 1–2 ml/min with BBS, which contained (in mM) 125 NaCl, 26 NaHCO₃, 2.5 KCl, 1.25 NaH₂PO₄, 2 CaCl₂, 1 MgCl₂, 10 glucose, and 0.2 d-tubocurarine, bubbled to pH 7.4 with 95% O₂ and 5% CO₂. Usually, a cleaning pipette was used to remove loose material from the cell surface. Conventional whole-cell recordings

(Hamill et al., 1981) were performed with 3–4 M$\Omega$ pipettes and an EPC-9 patch clamp amplifier, together with PULSE software (HEKA, Lambrecht, Germany). The pipette solution contained (in mM) 110 Cs-glutamate, 8 NaCl, 2 Mg-ATP, 0.3 Na$_2$-GTP, 20 Cs-HEPES, 5 nitrophenyl-EGTA, 3.5 CaCl$_2$, 0.3 Furaptra, and 0.2 Fura-2. This solution was titrated to pH 7.2, and its osmolality was 300 mOsm. Experiments were carried out at room temperature.

Capacitance measurements were performed using the Lindau-Neher technique, implemented as the "sine + dc" mode of the "software lock-in" extension of PULSE software. A 1 kHz, 70 mV peak-to-peak sinusoid stimulus was applied about a DC holding potential of −80 mV. Data were acquired through a combination of the high time resolution PULSE software and the lower time resolution X-Chart plug-in module to the PULSE software.

### Measurements of [Ca²⁺]ᵢ and Photolysis of Caged Ca²⁺

[Ca²⁺]ᵢ was measured by dual-wavelength ratiometric fluorimetry with a mixture of the indicator dyes Fura-2 and Furaptra. The dyes were excited with light alternated between 350 and 380 nm using a monochromator-based system (TILL Photonics, Planegg, Germany), and the resulting fluorescent signal was measured using a photomultiplier. To convert the ratio R of the fluorescent signals at both wavelengths into [Ca²⁺]ᵢ, a calibration curve was constructed, where each data point corresponds to the average ratio obtained during in vivo measurements using pipette solutions with free Ca²⁺ buffered to the respective concentrations (Figure 7). Whole-cell recordings where made on chromaffin cells, using pipette solutions containing (in mM) 8 NaCl; 2 Mg-ATP; 0.3 Na$_2$-GTP; 20 Cs-HEPES; 5 nitrophenyl-EGTA; 0.3 Furaptra; 0.2 Fura-2; 40 1,2-bis(2-aminophenoxy)ethane-N,N,N′,N′-tetraacetate (BAPTA); or 40 1,3-diaminopropane-2-ol-N,N′-tetraacetate (DPTA) and sufficient CaCl$_2$ to reach the indicated Ca²⁺ concentrations. This solution was supplemented with Cs-glutamate to reach a final osmolality of 300 mOsm. For the calculation of free [Ca²⁺] in these solutions, the Ca²⁺ dissociation constants ($K_D$) for DPTA, BAPTA, and NP-EGTA were assumed to be 81 $\mu$M, 221 nM, and 78 nM, respectively.

To obtain stepwise increases in [Ca²⁺]ᵢ, short flashes of ultraviolet light from a xenon arc flash lamp (Rapp OptoElectronics, Hamburg, Germany) were applied to the whole cell. The monochromator light was not only used to measure [Ca²⁺]ᵢ (see above) but also allowed to adjust [Ca²⁺]ᵢ before and after a flash, by photolysing smaller amounts of NP-EGTA.

### Analysis and Numerical Calculations

All experimental data were first analyzed with the program IgorPro (Wavemetrics, Lake Oswego, OR) and transferred to Origin 6.0 (Microcal Software, Northampton, MA) for further statistical analysis and display.

The differential equations describing the equilibrium between vesicle pools and the fusion kinetics were solved using a fifth-order Runge-Kutta integration scheme with adaptive step size. The downhill simplex method was used to find parameters that gave the best fit to the experimental results.

### Acknowledgments

### References

Ashery, U., Varoqueaux, F., Voets, T., Betz, A., Thakur, P., Koch, H., Neher, E., Brose, N., and Rettig, J. (2000). Munc13-1 acts as a priming factor for large dense-core vesicles in bovine chromaffin cells. EMBO J. *18*, 3586–3596.

Augustin, I., Rosenmund, C., Sudhof, T.C., and Brose, N. (1999). Munc13-1 is essential for fusion competence of glutamatergic synaptic vesicles. Nature *400*, 457–461.

Augustine, G.J., Burns, M.E., DeBello, W.M., Hilfiker, S., Morgan, J.R., Schweizer, F.E., Tokumaru, H., and Umayahara, K. (1999). Proteins involved in synaptic vesicle trafficking. J. Physiol. *520*, 33–41.

Bittner, M.A., and Holz, R.W. (1992). Kinetic analysis of secretion from permeabilized adrenal chromaffin cells reveals distinct components. J. Biol. Chem. *267*, 16219–16225.

Blank, P.S., Cho, M.S., Vogel, S.S., Kaplan, D., Kang, A., Malley, J., and Zimmerberg, J. (1998). Submaximal responses in calcium-triggered exocytosis are explained by differences in the calcium sensitivity of individual secretory vesicles. J. Gen. Physiol. *112*, 559–567.

Brose, N., Petrenko, A.G., Sudhof, T.C., and Jahn, R. (1992). Synaptotagmin: a calcium sensor on the synaptic vesicle surface. Science *256*, 1021–1025.

Brose, N., Rosenmund, C., and Rettig, J. (2000). Regulation of transmitter release by Unc-13 and its homologues. Curr. Opin. Neurobiol. *10*, 303–311.

Chen, Y.A., Scales, S.J., Patel, S.M., Doung, Y.C., and Scheller, R.H. (1999). SNARE complex formation is triggered by Ca2+ and drives membrane fusion. Cell *97*, 165–174.

Davis, A.F., Bai, J., Fasshauer, D., Wolowick, M.J., Lewis, J.L., and Chapman, E.R. (1999). Kinetics of synaptotagmin responses to Ca2+ and assembly with the core SNARE complex onto membranes. Neuron *24*, 363–376.

Dittman, J.S., and Regehr, W.G. (1998). Calcium dependence and recovery kinetics of presynaptic depression at the climbing fiber to Purkinje cell synapse. J. Neurosci. *18*, 6147–6162.

Fasshauer, D., Sutton, R.B., Brunger, A.T., and Jahn, R. (1998). Conserved structural features of the synaptic fusion complex: SNARE proteins reclassified as Q- and R-SNAREs. Proc. Natl. Acad. Sci. USA *95*, 15781–15786.

Fernandez-Chacon, R., and Südhof, T.C. (1999). Genetics of synaptic vesicle function: toward the complete functional anatomy of an organelle. Annu. Rev. Physiol. *61*, 753–776.

Geppert, M., Goda, Y., Hammer, R.E., Li, C., Rosahl, T.W., Stevens, C.F., and Südhof, T.C. (1994). Synaptotagmin I: a major Ca2+ sensor for transmitter release at a central synapse. Cell *79*, 717–727.

Gomis, A., Burrone, J., and Lagnado, L. (1999). Two actions of calcium regulate the supply of releasable vesicles at the ribbon synapse of retinal bipolar cells. J. Neurosci. *19*, 6309–6317.

Grynkiewicz, G., Poenie, M., and Tsien, R.Y. (1985). A new generation of Ca2+ indicators with greatly improved fluorescence properties. J. Biol. Chem. *260*, 3440–3450.

Heidelberger, R., Heinemann, C., Neher, E., and Matthews, G. (1994). Calcium dependence of the rate of exocytosis in a synaptic terminal. Nature *371*, 513–515.

Heinemann, C., Chow, R.H., Neher, E., and Zucker, R.S. (1994). Kinetics of the secretory response in bovine chromaffin cells following flash photolysis of caged Ca2+. Biophys. J. *67*, 2546–2557.

Kasai, H. (1999). Comparative biology of Ca2+-dependent exocytosis: implications of kinetic diversity for secretory function. Trends Neurosci. *22*, 88–93.

Konishi, M., Hollingworth, S., Harkins, A.B., and Baylor, S.M. (1991). Myoplasmic calcium transients in intact frog skeletal muscle fibers monitored with the fluorescent indicator furaptra. J. Gen. Physiol. *97*, 271–301.

Kusano, K., and Landau, E.M. (1975). Depression and recovery of transmission at the squid giant synapse. J. Physiol. *245*, 13–22.

Li, C., Ullrich, B., Zhang, J.Z., Anderson, R.G., Brose, N., and Sudhof, T.C. (1995). Ca(2+)-dependent and -independent activities of neural and non-neural synaptotagmins. Nature *375*, 594–599.

Lonart, G., and Südhof, T.C. (2000). Assembly of SNARE core complexes occurs prior to neurotransmitter release to set the readily-releasable pool of synaptic vesicles. J. Biol. Chem. *275*, 27703–27707.

Marqueze, B., Boudier, J.A., Mizuta, M., Inagaki, N., Seino, S., and

Seagar, M. (1995). Cellular localization of synaptotagmin I, II, and III mRNAs in the central nervous system and pituitary and adrenal glands of the rat. J. Neurosci. *15*, 4906–4917.

Moser, T., and Neher, E. (1997). Rapid exocytosis in single chromaffin cells recorded from mouse adrenal slices. J. Neurosci. *17*, 2314–2323.

Neher, E. (1998). Vesicle pools and Ca2+ microdomains: new tools for understanding their roles in neurotransmitter release. Neuron *20*, 389–399.

Plattner, H., Artalejo, A.R., and Neher, E. (1997). Ultrastructural organization of bovine chromaffin cell cortex-analysis by cryofixation and morphometry of aspects pertinent to exocytosis. J. Cell Biol. *139*, 1709–1717.

Scales, S.J., Chen, Y.A., Yoo, B.Y., Patel, S.M., Doung, Y.C., and Scheller, R.H. (2000). SNAREs contribute to the specificity of membrane fusion. Neuron *26*, 457–464.

Smith, C. (1999). A persistent activity-dependent facilitation in chromaffin cells is caused by Ca2+ activation of protein kinase C. J. Neurosci. *19*, 589–598.

Smith, C., Moser, T., Xu, T., and Neher, E. (1998). Cytosolic Ca2+ acts by two separate pathways to modulate the supply of release-competent vesicles in chromaffin cells. Neuron *20*, 1243–1253.

Stevens, C.F., and Wesseling, J.F. (1998). Activity-dependent modulation of the rate at which synaptic vesicles become available to undergo exocytosis. Neuron *21*, 415–424.

Sutton, R.B., Fasshauer, D., Jahn, R., and Brunger, A.T. (1998). Crystal structure of a SNARE complex involved in synaptic exocytosis at 2.4 Å resolution. Nature *395*, 347–353.

Thomas, P., Wong, J.G., Lee, A.K., and Almers, W. (1993). A low-affinity Ca2+ receptor controls the final steps in peptide secretion from pituitary melanotrophs. Neuron *11*, 93–104.

Voets, T., Neher, E., and Moser, T. (1999). Mechanisms underlying phasic and sustained secretion in chromaffin cells from mouse adrenal slices. Neuron *23*, 607–615.

Vogel, S.S., Blank, P.S., and Zimmerberg, J. (1996). Poisson-distributed active fusion complexes underlie the control of the rate and extent of exocytosis by calcium. J. Cell Biol. *134*, 329–338.

von Rüden, L., and Neher, E. (1993). A Ca-dependent early step in the release of catecholamines from adrenal chromaffin cells. Science *262*, 1061–1065.

Walent, J.H., Porter, B.W., and Martin, T.F. (1992). A novel 145 kd brain cytosolic protein reconstitutes Ca2+-regulated secretion in permeable neuroendocrine cells. Cell *70*, 765–775.

Wang, L.Y., and Kaczmarek, L.K. (1998). High-frequency firing helps replenish the readily releasable pool of synaptic vesicles. Nature *394*, 384–388.

Wei, S., Xu, T., Ashery, U., Kollewe, A., Matti, U., Antonin, W., Rettig, J., and Neher, E. (2000). Exocytotic mechanism studied by truncated and zero layer mutants of the C-terminus of SNAP-25. EMBO J. *19*, 1279–1289.

Xu, T., Rammner, B., Margittai, M., Artalejo, A.R., Neher, E., and Jahn, R. (1999). Inhibition of SNARE complex assembly differentially affects kinetic components of exocytosis. Cell *99*, 713–722.

Zucker, R.S. (1996). Exocytosis: a molecular and physiological perspective. Neuron *17*, 1049–1055.